Sensorless Control Strategy for Salient-Pole PMSM Based on Extended EMF in Rotating Reference Frame

Shigeo Morimoto, *Member, IEEE*, Keisuke Kawamoto, Masayuki Sanada, *Member, IEEE*, and Yoji Takeda, *Member, IEEE*

***Abstract*—This paper presents a novel sensorless control strategy for a salient-pole permanent-magnet synchronous motor (PMSM). A new model of a salient-pole PMSM using an extended electromotive force (EMF) in the rotating reference frame is utilized to estimate both position and speed. The extended EMF is estimated by a least-order observer, and the estimation position error is obtained from the extended EMF. Both estimated position and speed are corrected so that the position error becomes zero. The proposed system is very simple and the design procedure is easy and clear. Several experimental drive tests are demonstrated and the experimental results show the effectiveness of the proposed sensorless control system.**

***Index Terms*—Extended electromotive force, interior permanent-magnet synchronous motor, observer, salient-pole permanent-magnet synchronous motor, sensorless control.**

I. Introduction

THE permanent-magnet synchronous motor (PMSM) is widely used in many applications, such as high-performance variable-speed drives. In particular, an interior PMSM (IPMSM) can offer a high-efficiency drive by utilizing the reluctance torque and a constant-power operation by the flux-weakening technique. In order to control a stator current vector suitably and then achieve a high-performance drive, the information of rotor position and speed are necessary. In most variable-speed drives, some type of shaft sensor such as an optical encoder or resolver is connected to the rotor shaft. However, such sensor presents several disadvantages, such as drive cost, machine size, reliability, and noise immunity. Therefore, the sensorless control of an PMSM is desired, and various sensorless control strategies have been investigated [1]–[15].

Paper IPCSD 02–032, presented at the 2001 Industry Applications Society Annual Meeting, Chicago, IL, September 30–October 5, and approved for publication in the IEEE TRANSACTIONS ON INDUSTRY APPLICATIONS by the Industrial Drives Committee of the IEEE Industry Applications Society. Manuscript submitted for review October 15, 2001 and released for publication May 10, 2002.

S. Morimoto, M. Sanada, and Y. Takeda are with the Department of Electrical and Electronics Systems, College of Engineering, Osaka Prefecture University, Sakai 599-8531, Japan (e-mail: s.morimoto@ieee.org; sanada@gto.ees.osakafu-u.ac.jp; takeda@gto.ees.osakafu-u.ac.jp).

K. Kawamoto was with the Department of Electrical and Electronics Systems, College of Engineering, Osaka Prefecture University, Sakai 599-8531, Japan. He is now with Hitachi, Ltd., Hitachi, Japan.

Publisher Item Identifier 10.1109/TIA.2002.800777.

The sensorless control in a PMSM drive is fundamentally classified into two kinds of strategies: 1) fundamental excitation method and 2) saliency and signal injection method [1], [14]. In the saliency and signal injection method, the feature of a salient-pole PMSM such that the inductance varies depending on the rotor position is used to estimate the rotor position. A suitable test signal such as a high-frequency voltage or current component is injected from the inverter in order to detect inductance variation [2]–[6]. The position can be estimated even at standstill and low speeds by this method. On the other hand, the fundamental excitation method does not need any additional test signal and estimates the rotor position and speed from the stator voltages and currents. However, it is hard to estimate position at the low-speed region. The sensorless strategy proposed in this paper belongs to this fundamental excitation method. Various approaches in this category have been suggested. Some approaches are based on the estimation of the back electromotive force (EMF) or flux linkage due to permanent magnets by means of a state observer or an extended Kalman filter [7]–[11]. Other simple methods are based on the voltage or current error between the detected variables and the calculated variables from the motor model [12]–[14]. Most fundamental excitation methods are applied to a nonsalient-pole PMSM. Some approximations are necessary to apply such sensorless algorithms to the salient-pole PMSM. The approximation might cause the estimation error and the decrease in performance, and might make the system unstable in the worst case. A novel IPMSM model is obtained by using an extended EMF. The sensorless control scheme based on the model with the extended EMF in the stationary reference frame was proposed in [15], where the approximation is not required.

In the proposed strategy in this paper, the mathematical model of the IPMSM using the extended EMF in the rotating reference frame is utilized in order to estimate both position and speed. The extended EMF is estimated by a least-order observer, and the estimation position error is obtained from the extended EMF. The proposed scheme corrects the estimated position and speed so that the estimation position error becomes zero. The proposed system is very simple and the design procedure is easy and clear. Several experimental drive tests are demonstrated, where the current vector of the IPMSM is effectively controlled not only by a maximum torque-per-ampere control but also by a flux-weakening control over the base speed. The experimental results show the effectiveness of the proposed sensorless control system.

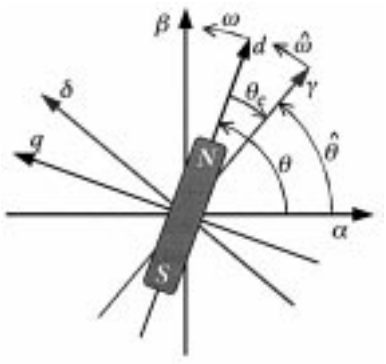

Fig. 1. Space-vector diagram of IPMSM.

II. Model of Salient-Pole PMSM

Fig. 1 shows the space-vector diagram of IPMSM, which indicates the relations of three reference frames used in this paper. The α–β frame is fixed to the stator winding and the α axis coincides with the u phase axis. The d–q frame corresponds to the synchronously rotating reference frame, and the d axis coincides with the *N* pole of the rotor. The voltage equation of a salient-pole PMSM such as an IPMSM in the stationary α–β frame is given as follows:

$$\begin{bmatrix} v_\alpha \\ v_\beta \end{bmatrix} = \begin{bmatrix} R_a + p(L_0 + L_1\cos 2\theta) & pL_1 \sin 2\theta \\ pL_1 \sin 2\theta & R_a + p(L_0 - L_1 \cos 2\theta) \end{bmatrix} \cdot \begin{bmatrix} i_\alpha \\ i_\beta \end{bmatrix} + \omega\psi_a \begin{bmatrix} -\sin\theta \\ \cos\theta \end{bmatrix} \quad (1)$$

where

i_α, i_β	α- and β-axes armature current;
v_α, v_β	α- and β-axis stator voltage;
ω	rotor angular velocity;
θ	rotor position;
R_a	armature resistance;
ψ_a	magnet flux linkage;

$$L_0 = \frac{L_d + L_q}{2}, \quad L_1 = \frac{L_d - L_q}{2},$$

L_d and L_q are the d- and q-axes inductances; and p is the differential operator.

The voltage equation in the rotating d–q reference frame is expressed as follows by transforming (1) into the d–q coordinate:

$$\begin{bmatrix} v_d \\ v_q \end{bmatrix} = \begin{bmatrix} R_a + pL_d & -\omega L_q \\ \omega L_d & R_a + pL_q \end{bmatrix} \begin{bmatrix} i_d \\ i_q \end{bmatrix} + \begin{bmatrix} 0 \\ \omega\psi_a \end{bmatrix} \quad (2)$$

where i_d and i_q are the d- and q-axes armature currents, and v_d and v_q are the d- and q-axes stator voltages.

The above d–q model is usually used for a high-performance PMSM drive. In the position-sensorless drive system, however, such d–q model cannot be utilized because the rotor position is not detected. The mathematical model in the estimated rotating γ–δ frame, which lags by θ_e from the d–q reference frame as shown in Fig. 1, is derived as follows by transforming (1) into the γ–δ frame:

$$\begin{bmatrix} v_\gamma \\ v_\delta \end{bmatrix} = \begin{bmatrix} R_a + pL_d & -\omega L_q \\ \omega L_d & R_a + pL_q \end{bmatrix} \begin{bmatrix} i_\gamma \\ i_\delta \end{bmatrix} + \begin{bmatrix} \varepsilon_\gamma \\ \varepsilon_\delta \end{bmatrix} \quad (3)$$

where

$$\begin{bmatrix} \varepsilon_\gamma \\ \varepsilon_\delta \end{bmatrix} = \omega\psi_a \begin{bmatrix} -\sin\theta_e \\ \cos\theta_e \end{bmatrix} + \boldsymbol{L_a} p \begin{bmatrix} i_\gamma \\ i_\delta \end{bmatrix} + \omega \boldsymbol{L_b} \begin{bmatrix} i_\gamma \\ i_\delta \end{bmatrix} + (\hat{\omega} - \omega)\boldsymbol{L_c} \begin{bmatrix} i_\gamma \\ i_\delta \end{bmatrix} \quad (4)$$

$$\boldsymbol{L_a} = \begin{bmatrix} -(L_d - L_q)\sin^2\theta_e & (L_d - L_q)\sin\theta_e\cos\theta_e \\ (L_d - L_q)\sin\theta_e\cos\theta_e & (L_d - L_q)\sin^2\theta_e \end{bmatrix} \quad (5)$$

$$\boldsymbol{L_b} = \begin{bmatrix} -(L_d - L_q)\sin\theta_e\cos\theta_e & -(L_d - L_q)\sin^2\theta_e \\ -(L_d - L_q)\sin^2\theta_e & (L_d - L_q)\sin\theta_e\cos\theta_e \end{bmatrix} \quad (6)$$

$$\boldsymbol{L_c} = \begin{bmatrix} (L_d - L_q)\sin\theta_e\cos\theta_e & -L_d\cos^2\theta_e - L_q\sin^2\theta_e \\ L_d\sin^2\theta_e + L_q\cos^2\theta_e & -(L_d - L_q)\sin\theta_e\cos\theta_e \end{bmatrix}. \quad (7)$$

It seems that the expression of (3) is the same as (2), however, the second term of each equation is quite different as shown in (4). The second and third terms in (4) become zero if the PMSM is a nonsalient-pole machine ($L_d = L_q$), but they are very complex in the salient-pole machine such as the IPMSM. In some sensorless control methods, such effects due to saliency are ignored.

The model in the d–q frame given by (2) can be rewritten as follows [15]:

$$\begin{bmatrix} v_d \\ v_q \end{bmatrix} = \begin{bmatrix} R_a + pL_d & -\omega L_q \\ \omega L_q & R_a + pL_d \end{bmatrix} \begin{bmatrix} i_d \\ i_q \end{bmatrix} + \begin{bmatrix} 0 \\ E_{ex} \end{bmatrix} \quad (8)$$

where

$$E_{ex} = \omega[(L_d - L_q)i_d + \psi_a] - (L_d - L_q)(pi_q). \quad (9)$$

The second term of (8) is called an extended EMF. Transforming this equation into the γ–δ frame, the following novel model in the rotating reference is obtained:

$$\begin{bmatrix} v_\gamma \\ v_\delta \end{bmatrix} = \begin{bmatrix} R_a + pL_d & -\omega L_q \\ \omega L_q & R_a + pL_d \end{bmatrix} \begin{bmatrix} i_\gamma \\ i_\delta \end{bmatrix} + \begin{bmatrix} e_\gamma \\ e_\delta \end{bmatrix} \quad (10)$$

where

$$\begin{bmatrix} e_\gamma \\ e_\delta \end{bmatrix} = E_{ex} \begin{bmatrix} -\sin\theta_e \\ \cos\theta_e \end{bmatrix} + (\hat{\omega} - \omega)L_d \begin{bmatrix} -i_\delta \\ i_\gamma \end{bmatrix}. \quad (11)$$

This model is very simple compared with (3) and it can be utilized by any type of synchronous motor such as a surface PMSM ($L_d = L_q$), interior PMSM ($L_d < L_q$), and synchronous reluctance motor ($\psi_a = 0$). The proposed sensorless scheme in this paper is based on this new mathematical model, where the approximation is not needed at all. The extended EMF in the rotating reference frame, which includes the information of estimation position error θ_e, is utilized for the estimation of rotor position and speed.

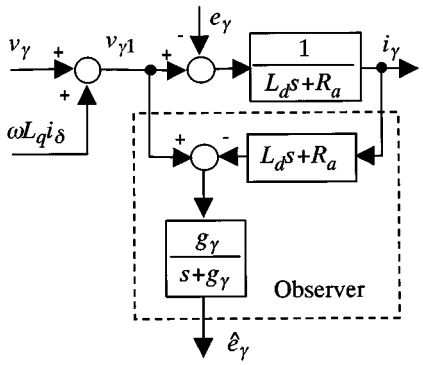

Fig. 2. Equivalent block diagram of least-order observer for estimation of extended EMF.

III. Estimation Algorithm

A. Estimation of Extended EMF

From the model of (10), the state-space equation for estimating the extended EMF is obtained when it is assumed that the differentiation of the time of the extended EMF is zero ($pe_\gamma = 0$ and $pe_\delta = 0$)

$$p\begin{bmatrix} i_\gamma \\ e_\gamma \end{bmatrix} = \frac{1}{L_d}\begin{bmatrix} -R_a & -1 \\ 0 & 0 \end{bmatrix}\begin{bmatrix} i_\gamma \\ e_\gamma \end{bmatrix} + \frac{1}{L_d}\begin{bmatrix} 1 \\ 0 \end{bmatrix} v_{\gamma 1} \quad (12)$$

$$p\begin{bmatrix} i_\delta \\ e_\delta \end{bmatrix} = \frac{1}{L_d}\begin{bmatrix} -R_a & -1 \\ 0 & 0 \end{bmatrix}\begin{bmatrix} i_\delta \\ e_\delta \end{bmatrix} + \frac{1}{L_d}\begin{bmatrix} 1 \\ 0 \end{bmatrix} v_{\delta 1} \quad (13)$$

where

$$\left.\begin{aligned} v_{\gamma 1} &= v_\gamma + \omega L_q i_\delta \\ v_{\delta 1} &= v_\delta - \omega L_q i_\gamma \end{aligned}\right\}. \quad (14)$$

The input voltages are compensated in order to eliminate the cross coupling between the γ- and δ-axes as shown in (14). Thus, the state-space equation is decoupled and becomes simple as (12) and (13). The extended EMF can be easily estimated by a least-order observer. Fig. 2 shows the equivalent block diagram of the least-order observer for estimating e_γ, where g_γ represents the gain of the observer. The δ-axis component of the extended EMF e_δ is also estimated in the same way as e_γ. Assuming that the error between the estimated speed $\hat{\omega}$ and the actual speed ω is sufficiently small, the extended EMF is estimated as follows:

$$\begin{bmatrix} \widehat{e}_\gamma \\ \widehat{e}_\delta \end{bmatrix} = E_{ex}\begin{bmatrix} -\sin\widehat{\theta}_e \\ \cos\widehat{\theta}_e \end{bmatrix}. \quad (15)$$

B. Estimation of Speed and Position

From the estimated extended EMF ($\widehat{e}_\gamma$ and $\widehat{e}_\delta$), the estimation position error $\widehat{\theta}_e$ can be derived by the following two ways:

Scheme A:

$$\widehat{\theta}_e = \tan^{-1}\left(-\frac{\widehat{e}_\gamma}{\widehat{e}_\delta}\right) \quad (16)$$

Scheme B:

$$\widehat{\theta}_e \cong \left(\frac{-\widehat{e}_\gamma}{E_{ex}}\right). \quad (17)$$

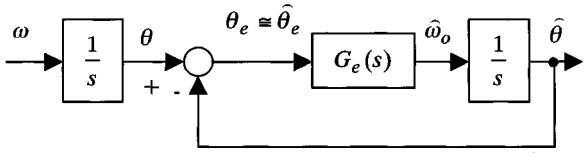

Fig. 3. Equivalent block diagram of position and speed estimator.

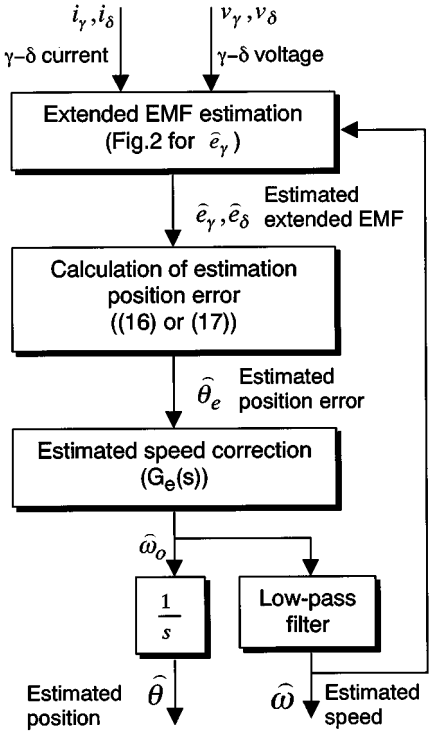

Fig. 4. Block diagram of position and speed estimation algorithm.

The estimated speed $\widehat{\omega}_o$ and the estimated position $\widehat{\theta}$ are compensated by compensator $G_e(s)$ so that the position error becomes zero. This scheme can be comparatively represented as a simple feedback system as shown in Fig. 3. The estimated position $\widehat{\theta}$ follows the actual one as (18) when the proportional and integral (PI) compensator is selected as $G_e(s)$

$$\widehat{\theta} = \frac{K_{ep}s + K_{ei}}{s^2 + K_{ep}s + K_{ei}}\theta. \quad (18)$$

K_{ep} and K_{ei} in (18) are proportional and integral gains. The estimating performance is designed only by the PI gains of K_{ep} and K_{ei}. When the natural frequency ω_n and the damping ratio ζ_n in the feedback system in Fig. 3 are designed, the PI gains are automatically determined by

$$K_{ep} = 2\zeta_n\omega_n, \quad K_{ei} = \omega_n^2. \quad (19)$$

The transfer function from the actual speed ω to the estimated speed $\widehat{\omega}_o$ is the same as that from θ to $\widehat{\theta}$ given by (18).

The position and speed estimation algorithm is summarized as shown in Fig. 4. In practical use, the estimated speed $\widehat{\omega}_o$ is filtered through a low-pass filter to reduce the influence of noise. The filtered estimated speed $\widehat{\omega}$ is used to motor control

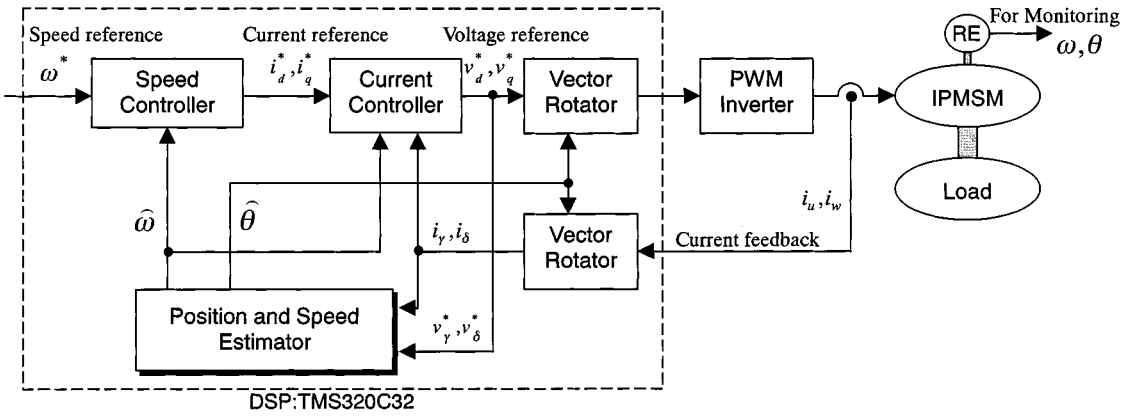

Fig. 5. Block diagram of proposed sensorless speed control system.

TABLE I
SPECIFICATIONS OF TESTED IPMSM

Number of pole pairs	2	
Rated (base) speed	2000	r/min
Rated Torque	1.77	Nm
Rated phase current	5.0	A
Armature resistance R_a	0.824	Ω
Magnet flux-linkage ψ_a	0.0785	Wb
d- axis inductance L_d	9.67	mH
q-axis inductance L_q	Equation (20)	

and estimation of extended EMF. The proposed algorithm is of simple structure and the process of design is clear and easy.

IV. EXPERIMENTAL RESULTS

A. Experimental Test Setup

Fig. 5 shows the block diagram of the proposed sensorless speed control system. The specifications of the tested IPMSM are listed in Table I. The q-axis inductance L_q of the IPMSM usually varies due to the magnetic saturation. The variation of L_q is considered by (20) in the experiments

$$L_q = 0.0243 - 0.0007 i_\delta. \tag{20}$$

The position estimation error occurs although the speed estimation error is not caused when there is an error of q-axis inductance between a motor model and actual motor. The control system might become unstable when the error of the motor parameter is very large. The control algorithms are implemented on a Texas Instruments TMS320C32 floating-point digital signal processor (DSP). The sampling period is 5 ms for speed control and 0.1 ms for the other control parts, including the speed and position estimation. The speed controller generates the d- and q-axes current references i_d^* and i_q^*. The q-axis current reference i_q^* is produced by a PI compensator according to the speed error and the d-axis current reference i_d^* is determined by the current vector control algorithm such as a maximum torque-per-ampere control and a flux-weakening control [16]. In the experiments, the current vector is controlled by the maximum torque-per-ampere control below the base speed of 2000 r/min and by the flux-weakening control above the base speed.

The observer gain is selected as $g_\gamma = g_\delta = 600$, which corresponds to the cutoff frequency of a first-order low-pass filter in the observer which is 600 rad/s. The PI compensator in the estimated speed correction is designed as $\omega_n = 45$ rad/s and $\zeta_n = 0.5$. The cutoff frequency of a low-pass filter in the speed estimation is selected as 100 rad/s. Scheme A given by (16) is applied for the calculation of position estimation error in the experiments of Sections IV-B and C.

B. Steady-State Performance

Fig. 6 shows the steady-state performance at rating (2000 r/min, 1.77 N·m). Both an estimation position error and an estimation speed error are very small and, as a result, the high-performance drive equal to that using the position sensor can be achieved by the proposed sensorless control.

Fig. 7 shows the steady-state torque–speed characteristics. The flux-weakening control is applied above the base speed of 2000 r/min in order to control the stator voltage within the ceiling voltage and, thus, the constant-power operation is achieved over twice rated speed. The speed range below the base speed is the constant-torque region. The speed fluctuation becomes large as the speed decreases below 200 r/min. The operation at 100 r/min with about 40% load has been confirmed, but a stable operation cannot be obtained below 100 r/min.

In the proposed method, which is a kind of fundamental excitation method, the effective information of voltage and current vanishes as the speed decreases, and the estimation performance deteriorates just as in other kinds of the fundamental excitation method. In order to drive to lower speed, the accurate voltage and current information, an accurate motor model and its parameters are necessary. In the proposed method, the position estimation at standstill is impossible just as in other kinds of the fundamental excitation method. Therefore, it is necessary to apply other methods such as a saliency and signal injection method to estimate the initial rotor position and drive the motor at lower speed. In the other starting method, by the open-loop V/F control method, the motor is also accelerated up to the speed where the proposed sensorless method can estimate the rotor position.

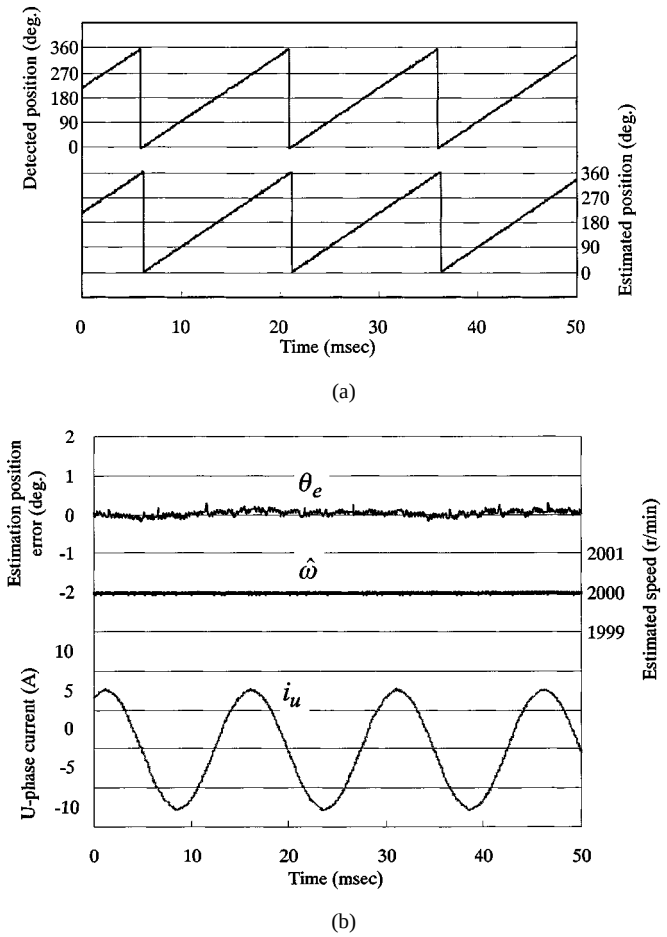

Fig. 6. Steady-state performance of proposed sensorless drive at rating. (a) Detected position and estimated position. (b) Estimation position error, estimated speed, and current.

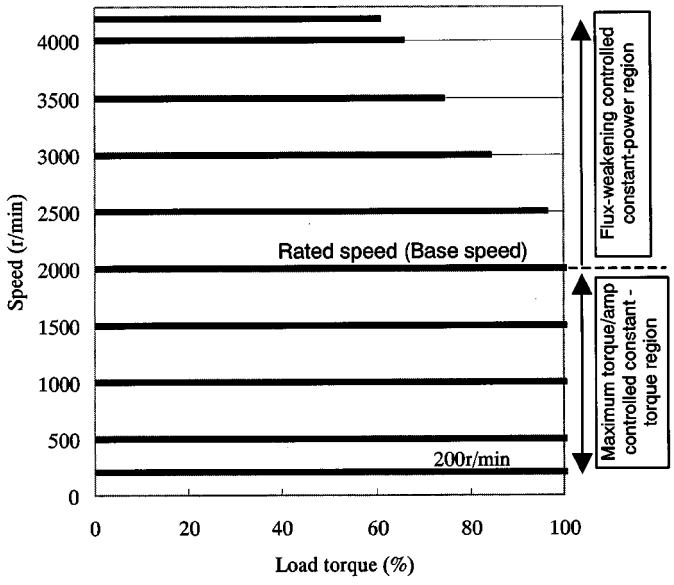

Fig. 7. Steady-state torque–speed characteristics.

C. Transient Performance

Fig. 8 shows the responses for step change of speed reference. The estimation position error θ_e ($=\theta - \hat{\theta}$) and the estimation speed error ($\omega - \hat{\omega}$) are sufficiently small and good speed response is achieved.

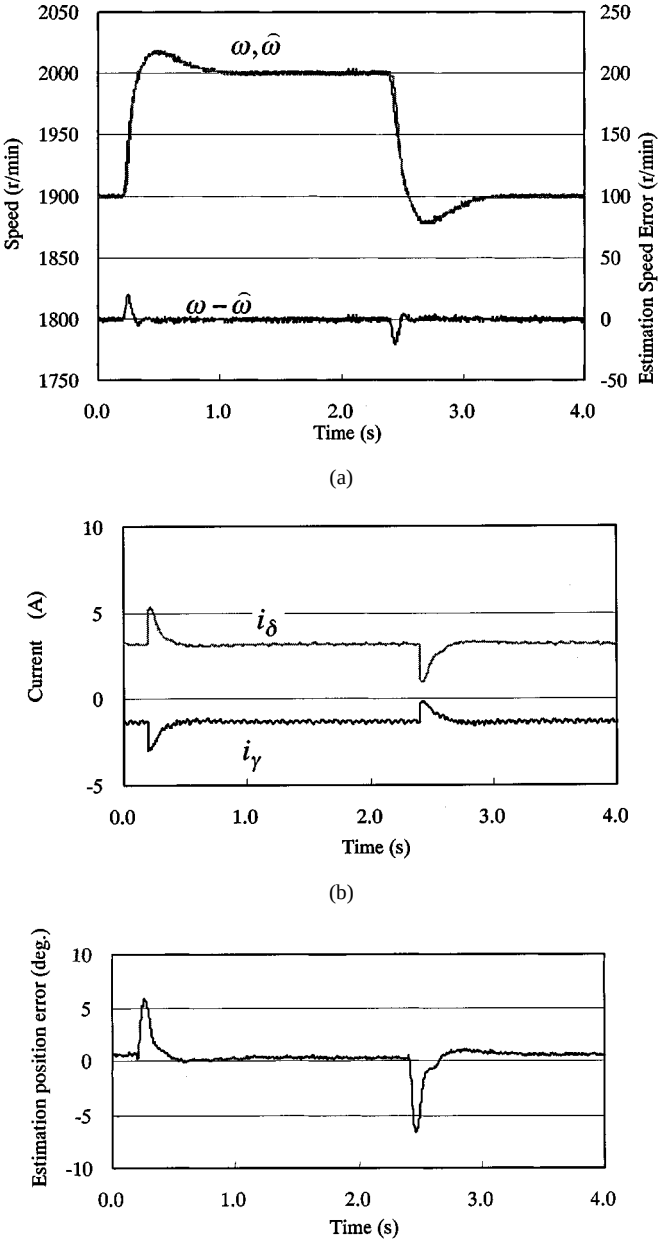

Fig. 8. Responses for step change of speed reference (1900 → 2000 → 1900 r/min, 28% load). (a) Detected speed, estimated speed, and estimation speed error. (b) γ- and δ-axes currents. (c) Estimation position error.

Fig. 9 shows the responses for a step change of 100% load torque. The estimation position error and estimation speed error reach 15° and 40 r/min, respectively, when the load changes rapidly, but they decrease at once. Good performance against load disturbance is obtained.

Fig. 10 shows the acceleration performance from 500 to 4000 r/min, which corresponds to twice the base speed. Below the base speed of 2000 r/min, the current vector is controlled in order to produce the maximum torque under the current limitation, thus, the motor is accelerated by the maximum

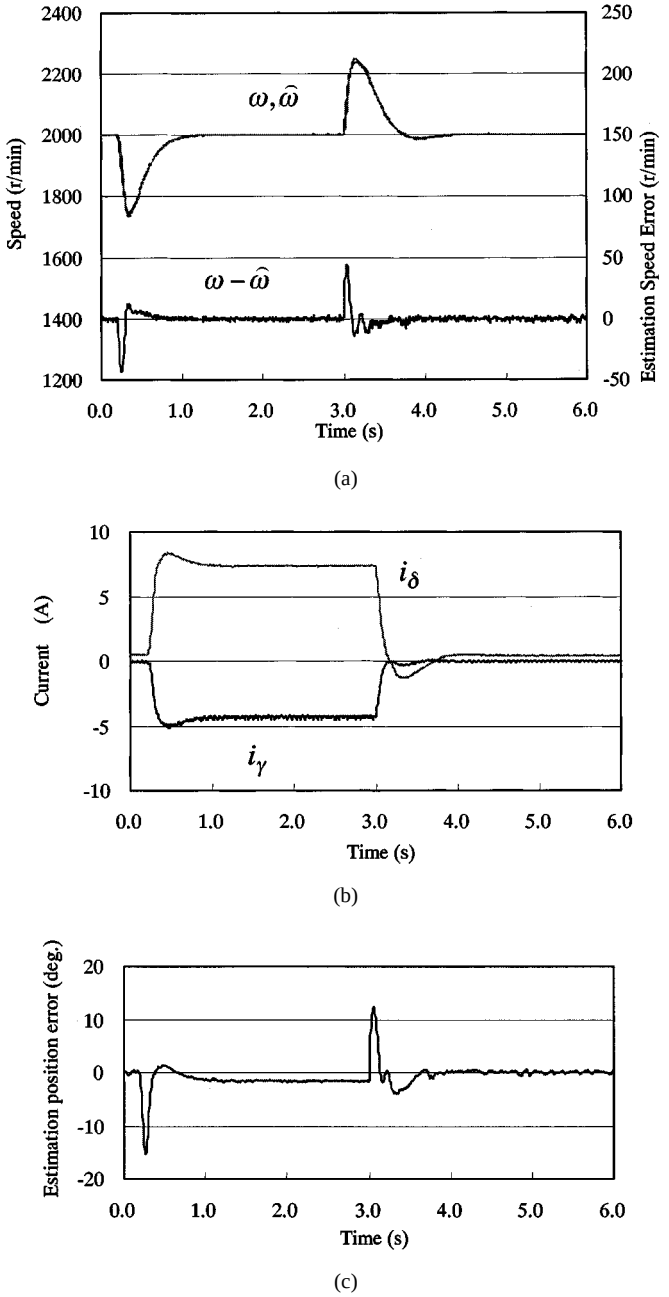

Fig. 9. Responses for step change of load torque (Speed reference: 2000 r/min, Load: 0 → 100% → 0). (a) Detected speed, estimated speed and estimation speed error. (b) γ- and δ-axis currents. (c) Estimation position error.

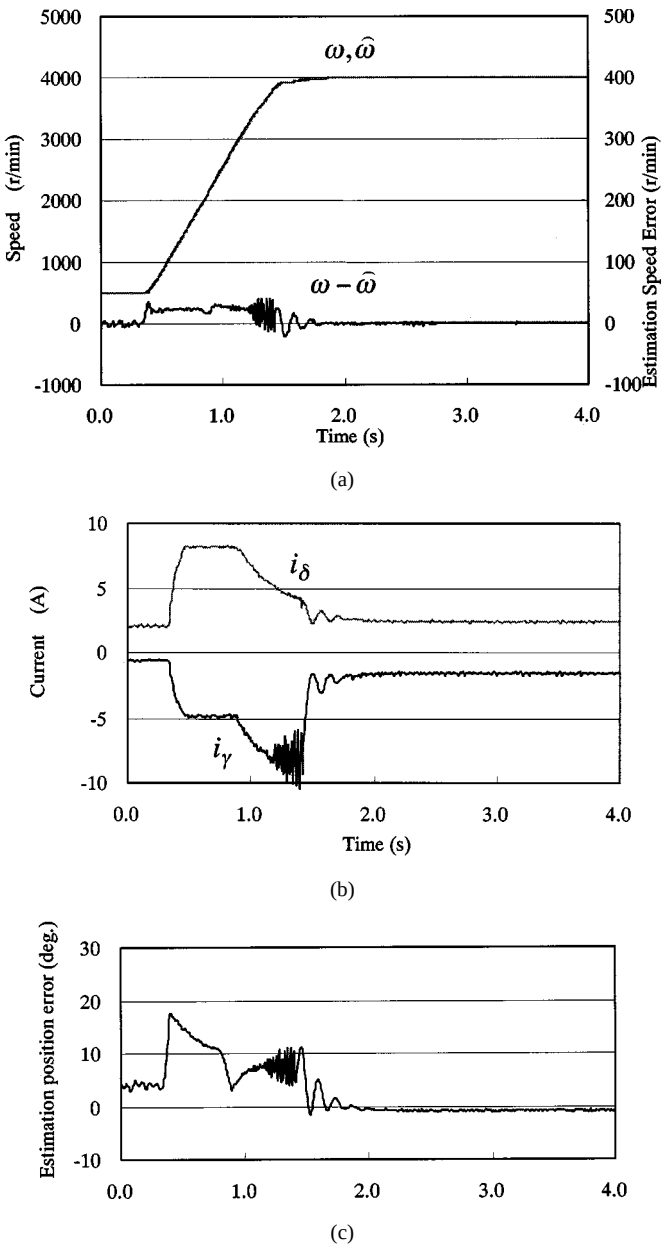

Fig. 10. Acceleration performance from 500 to 4000 r/min by flux-weakening control. (a) Detected speed, estimated speed, and estimation speed error. (b) γ- and δ-axes currents. (c) Estimation position error.

available torque. The stator voltage exceeds the maximum available voltage of the inverter above the base speed and, thus, the current controller is saturated. Avoiding voltage saturation, the flux-weakening control is applied over the base speed. The current vector is effectively controlled according to the motor speed, and the transition from the maximum torque-per-ampere control to the flux-weakening control has been smoothly achieved as shown in Fig. 10. Good accelerating performance from low speed to high speed is achieved. The estimation position error over 10° appears during acceleration in Fig. 10. It can be reduced by changing the compensator $G_e(s)$ in the speed and position estimator. When $G_e(s)$ is selected as (21), the transfer function from the actual rotor position to the estimated position becomes (22), and the decrease of estimation error during acceleration is expected

$$G_e(s) = K_1 + \frac{K_2}{s} + \frac{K_3}{s^2} \tag{21}$$

$$\hat{\theta} = \frac{K_1 s^2 + K_2 s + K_3}{s^3 + K_1 s^2 + K_2 s + K_3}\,\theta. \tag{22}$$

Fig. 11 shows the experimental results of the same drive test of Fig. 10, where the compensator of (21) is used and three gains in (21) are determined so as to satisfy the following condition:

$$s^3 + K_1 s^2 + K_2 s + K_3 = (s+\omega_n)(s^2 + 2\zeta_n \omega_n s + \omega_n^2). \tag{23}$$

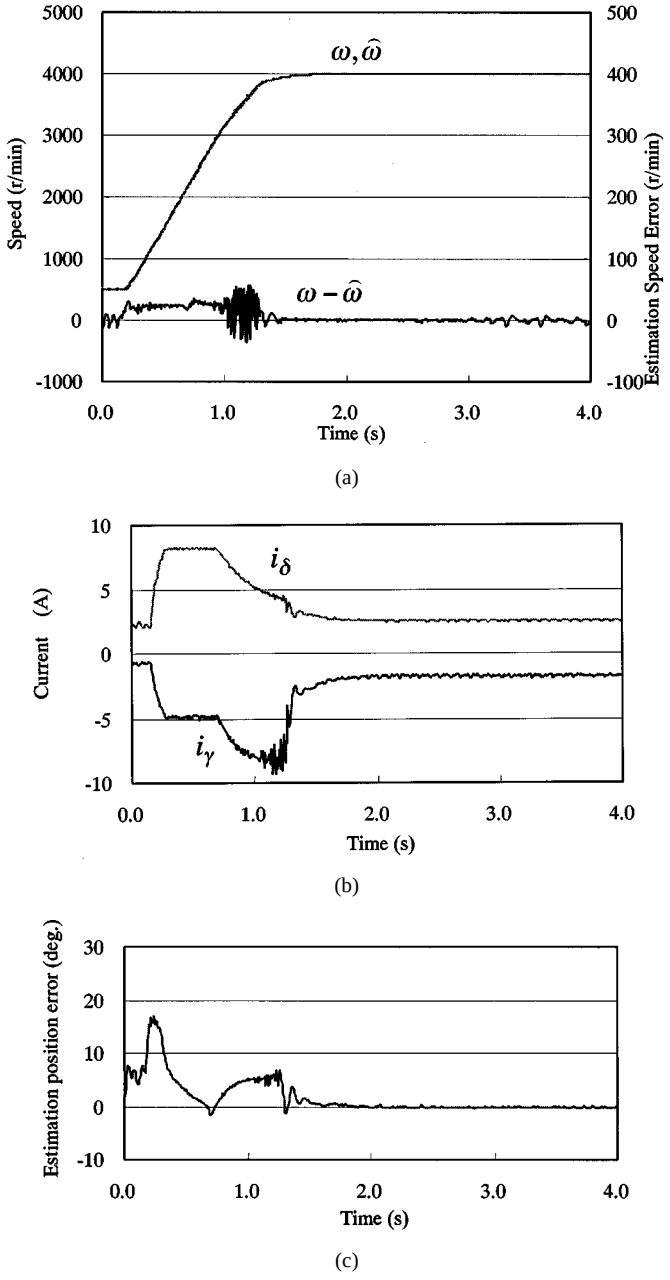

Fig. 11. Acceleration performance from 500 r/min to 4000 r/min with compensator of (21). (a) Detected speed, estimated speed and estimation speed error. (b) γ- and δ-axis currents. (c) Estimation position error.

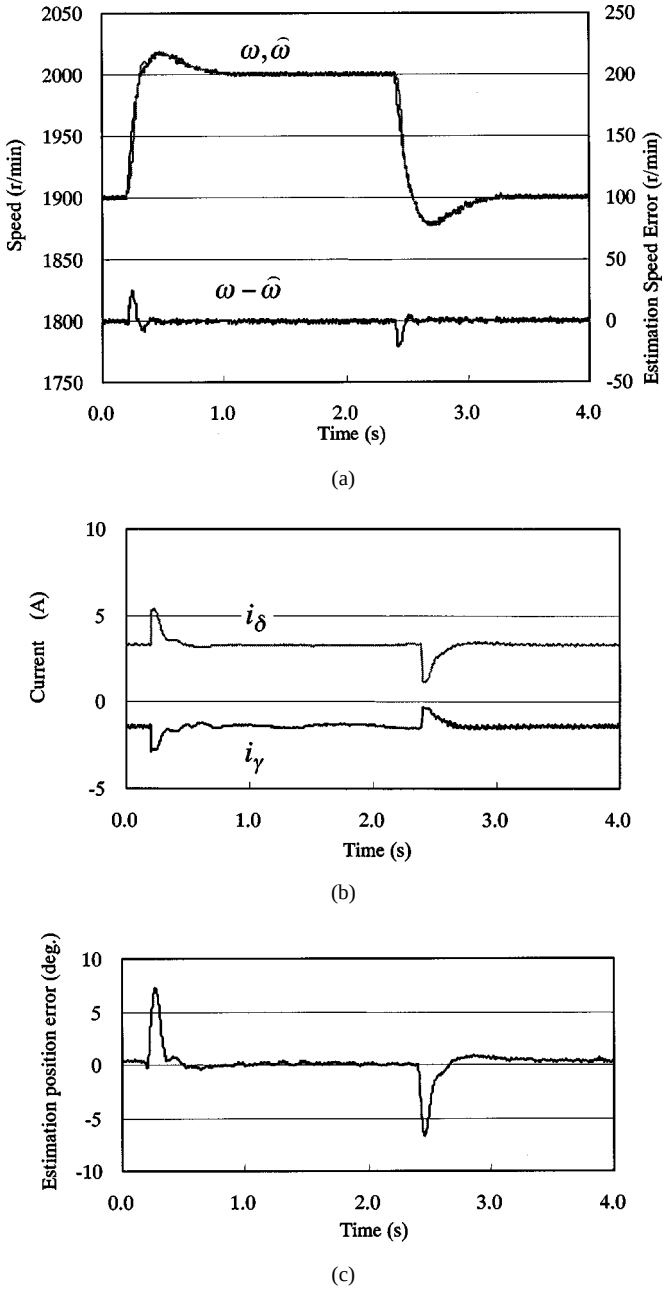

Fig. 12. Operating performance of simplified algorithm (1900 → 2000 → 1900 r/min, 28% load). (a) Detected speed, estimated speed, and estimation speed error. (b) γ- and δ-axes currents. (c) Estimation speed error.

ω_n and ζ_n are the same values as in the foregoing experiments ($\omega_n = 45$ rad/s, $\zeta_n = 0.5$). The effect of reducing estimation position error during acceleration is confirmed.

D. Simplification of Sensorless System

It is possible to make the speed and position estimator simpler by using Scheme B for calculation of estimation position error, where the position estimation error is assumed to be small enough. The estimation position error is calculated as follows by applying some approximation to (9) and (17):

$$\widehat{\theta}_e = \frac{-\hat{e}_\gamma}{\widehat{\omega}\left[(L_d - L_q)i_\gamma + \psi_a\right]}. \tag{24}$$

The γ-axis component of the extended EMF is estimated as only one least-order observer shown in Fig. 2. The algorithm of estimating speed and rotor position is the same after the estimation position error is calculated by (24).

Fig. 12 shows the performance of this simplified algorithm, where the change of speed reference is the same as in Fig. 8. It seems that the estimation position error and speed error are somewhat increasing compared with Fig. 8, however, good operating performance is obtained.

V. Conclusions

This paper has proposed a novel sensorless control strategy for a salient-pole PMSM, which is based on a novel motor

model in the rotating reference frame with an extended EMF. The sensorless drive system was implemented on a DSP and several drive tests were carried out. When the speed reference or the load torque changes rapidly, the position estimation error and the speed estimation error are caused. However, such errors are very small, and their influence on the motor drives is little. The effective current vector control strategy including a flux-weakening control over the base speed was applied to the IPMSM sensorless drive, and it has been confirmed that the proposed sensorless control strategy is effective for the salient-pole PMSM drives.

REFERENCES

[1] J. P. Johnson, M. Ehsani, and Y. Guzelgunler, "Review of sensorless methods for brushless DC," in *Conf. Rec. IEEE-IAS Annu. Meeting*, 1999, pp. 143–150.

[2] M. Schroedl, "Sensorless control of AC machines at low speed and standstill based on the 'INFORM' method," in *Conf. Rec. IEEE-IAS Annu. Meeting*, 1996, pp. 270–277.

[3] M. W. Degner and R. D. Lorenz, "Using multiple saliencies for the estimation of flux, position, and velocity in AC machines," in *Conf. Rec. IEEE-IAS Annu. Meeting*, 1997, pp. 760–767.

[4] S. Ogasawara and H. Akagi, "Implementation and position control performance of a position-sensorless IPM motor drive system based on magnetic saliency," *IEEE Trans. Ind. Applicat.*, vol. 34, pp. 806–812, July/Aug. 1998.

[5] R. Mizutani, T. Takeshita, and N. Matsui, "Current model-based sensorless drives of salient-pole PMSM at low speed and standstill," *IEEE Trans. Ind. Applicat.*, vol. 34, pp. 841–846, July/Aug. 1998.

[6] L. Wang and R. D. Lorenz, "Rotor position estimation for permanent magnet synchronous motor using saliency-tracking self-sensing method," in *Conf. Rec. IEEE-IAS Annu. Meeting*, 2000, pp. 445–450.

[7] R. Wu and G. R. Slemon, "A permanent magnet motor drive without a shaft sensor," *IEEE Trans. Ind. Applicat.*, vol. 27, pp. 1005–1011, Sept./Oct. 1991.

[8] N. Ertugrul and P. Acarnley, "A new algorithm for sensorless operation of permanent magnet motors," *IEEE Trans. Ind. Applicat.*, vol. 30, pp. 126–133, Jan./Feb. 1994.

[9] J. Kim and S. Sul, "High performance PMSM drives without rotational position sensors using reduced order observer," in *Conf. Rec. IEEE-IAS Annu. Meeting*, 1995, pp. 75–82.

[10] S. Bolognani, R. Oboe, and M. Zigliotto, "Sensorless full-digital PMSM drive with EKF estimation of speed and rotor position," *IEEE Trans. Ind. Electron.*, vol. 46, pp. 184–191, Feb. 1999.

[11] D. Yousfi, M. Azizi, and A. Saad, "Rotor position and speed estimation algorithm for permanent magnet synchronous drives," in *Conf. Rec. IEEE-IAS Annu. Meeting*, 2000, pp. 1541–1546.

[12] N. Matsui, "Sensorless PM brushless DC motor drives," *IEEE Trans. Ind. Electron.*, vol. 43, pp. 300–308, Apr. 1988.

[13] C. Bruguier, G. Champenois, and J. P. Rognan, "Current-model controls of a synchronous motor without position and speed sensors," in *Proc. IPEC-Yokohama'95*, 1995, pp. 1302–1308.

[14] L. Harnefor and H. P. Nee, "A general algorithm for speed and position estimation of AC motors," *IEEE Trans. Ind. Electron.*, vol. 47, pp. 77–83, Feb. 2000.

[15] Z. Chen, M. Tomita, S. Ichikawa, S. Doki, and S. Okuma, "Sensorless control of interior permanent magnet synchronous motor by estimation of an extended electromotive force," in *Conf. Rec. IEEE-IAS Annu. Meeting*, 2000, pp. 1814–1819.

[16] S. Morimoto, M. Sanada, and Y. Takeda, "Effects and compensation of magnetic saturation in flux-weakening controlled permanent magnet synchronous motor drives," *IEEE Trans. Ind. Applicat.*, vol. 30, pp. 1632–1637, Nov./Dec. 1994.

Shigeo Morimoto (M'93) was born in Japan in 1959. He received the B.E., M.E., and Ph.D. degrees from Osaka Prefecture University, Sakai, Japan, in 1982, 1984, and 1990, respectively.

He joined Mitsubishi Electric Corporation, Tokyo, Japan, in 1984. Since 1988, he has been with the Department of Electrical and Electronic Systems, Osaka Prefecture University, where he is currently an Associate Professor. He has been engaged in research on ac drive systems and motion control.

Dr. Morimoto is a member of the Institute of Electrical Engineers of Japan, Society of Instrumental and Control Engineers of Japan, Institute of Systems, Control and Information Engineers, and Japan Society for Power Electronics.

Keisuke Kawamoto was born in Japan in 1977. He received the B.E. and M.E. degrees from Osaka Prefecture University, Sakai, Japan, in 2000 and 2002, respectively.

He was involved in the study on the sensorless control of an IPMSM at Osaka Prefecture University. He is currently with Hitachi, Ltd., Hitachi, Japan.

Masayuki Sanada (M'94) was born in Japan in 1966. He received the B.E., M.E., and Ph.D. degrees from Osaka Prefecture University, Sakai, Japan, in 1989, 1991, and 1994, respectively.

In 1994, he joined the Department of Electrical and Electronic Systems, Osaka Prefecture University, where he is currently an Assistant Professor. His main research interests are linear motors for direct-drive applications and their control systems.

Dr. Sanada is a member of the Institute of Electrical Engineers of Japan, Japan Society for Power Electronics, and Japan Society of Applied Electromagnetics and Mechanics.

Yoji Takeda (M'93) was born in Osaka, Japan, in 1943. He received the B.E., M.E., and Ph.D. degrees from Osaka Prefecture University, Sakai, Japan, in 1966, 1968, and 1977, respectively.

In 1968, he joined the Department of Electrical and Electronic Systems, Osaka Prefecture University, where he is currently a Professor. His main research interests are permanent-magnet synchronous motors, linear motors, and their control systems.

Dr. Takeda is a member of the Institute of Electrical Engineers of Japan, Institute of Systems, Control and Information Engineers, and Japan Society for Power Electronics.